Published in Applied Physics Letters 78, 396-398, 2001
which should be used for any reference to this work

High-temperature operation of distributed feedback quantum-cascade lasers at 5.3 μm

Daniel Hofstetter,[a] Mattias Beck, Thierry Aellen, and Jérôme Faist
University of Neuchâtel, Institute of Physics, Rue A.-L. Breguet 1, CH-2000 Neuchâtel, Switzerland

High-temperature operation of a low-threshold 5.3 μm quantum-cascade distributed feedback laser is presented. The emission spectrum was single mode with more than 20 dB side mode suppression ratio for all investigated temperatures and up to thermal rollover. For 1.5% duty cycle and at 0 °C, the laser emitted 1.15 W of single mode peak power; at 120 °C, a value of 92 mW was seen. For a 3 mm long device, we observed a room-temperature threshold current density of 3.6 kA/cm^2. This remarkable performance is mainly due to a 4 quantum-well active region using a double phonon resonance for the lower laser level.

Distributed feedback (DFB) quantum-cascade (QC) lasers have proven to be very interesting light sources for the so-called atmospheric window regions both around 5 and 10 μm. Their main application potential lies in IR spectroscopy experiments such as photoacoustic spectroscopy,[1,2] and single-pass or multiple-pass absorption spectroscopy.[3,4] For these applications, properties like high output power, low power consumption, room-temperature operation, and a large single-mode tuning range are key features.[5,6] Since continuous-wave operation of QC lasers is not yet possible at room temperature, one has to pursue high average powers under pulsed current injection.[7] So far, high output powers were mainly a privilege of superlattice QC lasers. However, their major advantage, namely the short lifetime of the lower laser level, was usually obtained at the cost of a slightly worse injection efficiency. In this letter, we report 5.3 μm DFB lasers with a 4 quantum-well (QW) active region which combines the good injection efficiency of the diagonal anticrossed 3 QW design and the short ground state lifetime of the superlattice QC laser. The three lower states of the active region are designed to be separated by one phonon energy each. As a last point, a larger conduction band discontinuity, achieved by the use of strain-compensated InGaAs/InAlAs material,[8] helped to decrease the tunneling probability from the upper lasing state into the continuum.[9] All these changes resulted in an exceptionally low threshold current density and an excellent high-temperature performance up to 393 K (120 °C).

Fabrication of these devices relied on molecular-beam epitaxy of strain-compensated $In_{0.6}Ga_{0.4}As/In_{0.44}Al_{0.56}As$ layers on top of an n-doped InP (Si, 2×10^{17} cm^{-3}) substrate. The growth process started with the lower waveguide layers ($In_{0.53}Ga_{0.47}As$, Si, 6×10^{16} cm^{-3}, thickness 0.34 μm), proceeded with the active layers (Si, thickness 1.43 μm) and was finished by a thicker set of upper waveguide layers ($In_{0.53}Ga_{0.47}As$, Si, 6×10^{16} cm^{-3}, thickness 0.5 μm) and a highly n-doped cap layer ($In_{0.53}Ga_{0.47}As$, Si, 2×10^{18} cm^{-3}, thickness 0.4 μm) on top. This cap layer was also the host layer for the grating, as reported earlier.[10,11] Current injection into the grating layer was accomplished laterally through narrow metal stripes on the shoulders of the waveguide. This waveguide design has the advantages of being simple (no epitaxial regrowth), offering a strong coupling coefficient, and, finally, resulting in small absorption losses. The central portion of the waveguide consisted of 28 periods; each one of the latter contained an active region and an injector region, separated by an injection and an exit barrier. A schematic conduction band diagram of one period of the active layers is shown in Fig. 1. The upper and lower lasing states are the wave functions with numbers 4 and 3, respectively; and the ground state of the injector is denominated with the letter ''g.'' As already mentioned in the introduction, the active region was composed of 4 QWs which results in 3

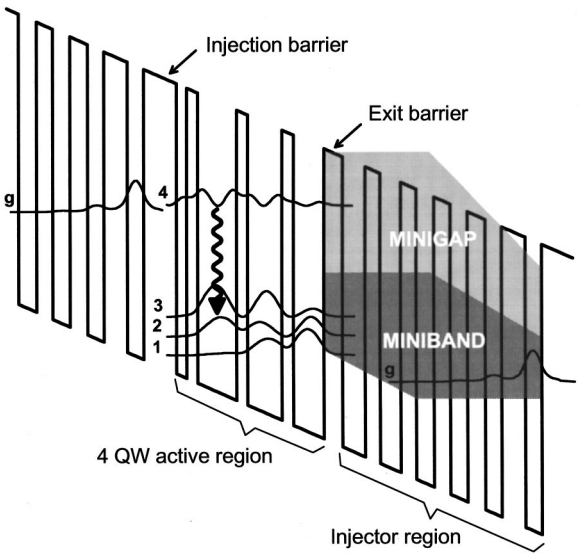

FIG. 1. Schematic conduction band diagram of a portion of the active layers and moduli squared of the relevant wave functions of a 5.3 μm QC laser with a 4 QW active layers. An electric field of 7.5×10^4 V/cm was applied to align the structure. The $In_{0.6}Ga_{0.4}As/In_{0.44}Al_{0.56}As$ layer sequence of one period of the active layers, starting from the injection barrier is as follows: **42**/13/**14**/50/**14**/44/**15**/39/**24**/29/**19**/26/**20**/23/**21**/22/**23**/21/**30**/21. Thicknesses are in angstroms, $In_{0.44}Al_{0.56}As$ barrier layers in bold, $In_{0.6}Ga_{0.4}As$ QW layers are in roman, doped layers (Si, 4×10^{17} cm^{-3}) are underlined.

[a]Electronic mail: Daniel.Hofstetter@unine.ch

coupled lower states (levels 1, 2, and 3). Each two of the latter (i.e., level 3→2, and level 2→1) were separated by one phonon energy. This double phonon resonance yielded a short intersubband electron scattering time $\{\tau_{32}=0.31\,\text{ps}$, $\tau_{31}=1.24\,\text{ps}$, $\tau_{\text{low}}=[(\tau_{32})^{-1}+(\tau_{31})^{-1}]^{-1}=0.25\,\text{ps}\}$ and therefore an efficient extraction of the electrons into the injector region. The upper lasing state exhibits a much longer intersubband electron scattering time of $\tau_{\text{up}}=[(\tau_{43})^{-1}+(\tau_{42})^{-1}+(\tau_{41})^{-1}]^{-1}=1.25\,\text{ps}$ (using $\tau_{43}=3.41\,\text{ps}$, $\tau_{42}=3.26\,\text{ps}$, and $\tau_{41}=5.07\,\text{ps}$). The relatively large dipole matrix element, $\langle z_{43}\rangle=2.1\,\text{nm}$, confirms that the lasing transition is mainly a vertical one. Thanks to the thin first well, which reduces the overlap of the injector ground state g with the lower lasing state wave functions 1, 2, and 3, the injection efficiency was kept similarly high as in the classical 3 QW design. The design takes thus advantage of the good properties of both the 3 QW design (high injection efficiency) and the superlattice design (short lifetime of the lower lasing state). In addition, the use of strain-compensated material makes the barrier height considerably larger (620 meV instead of 520 meV like for unstrained material), which quite efficiently reduces electron tunneling from the upper lasing state into the continuum. Finally, all wells can be made somewhat thicker, which has a positive effect on the interfacial roughness scattering. This is consistent with the relatively narrow linewidth of the luminescence peak measured at 4 K ($h\nu=244\,\text{meV}$, $\Delta E=11\,\text{meV}$) and at 300 K ($h\nu=233\,\text{meV}$, $\Delta E=25\,\text{meV}$).

The fabrication process started by holographically defining a grating with 0.825 μm period ($n_{\text{eff}}=3.21$), and wet chemical etching of the grating to a depth of 100 nm in a $H_3PO_4/H_2O_2/H_2O$ solution (4:1:10, etch rate 800 nm/min). We used a 488 nm Ar-ion laser and a 90° corner reflector mounted on a rotational stage for the grating exposure. Wet chemical etching in a $HBr/HNO_3/H_2O$ solution (1:1:10, etch rate 800 nm/min) was then used to define broad ridge waveguides with a width of 44 μm (etch depth 5 μm) and a length of 3 mm. 300 nm of Si_3N_4 served as an electrical passivation layer and Ti/Au (10/1000 nm) was used as top contact metal. Thinning, backcontacting (Ge/Au/Ag/Au, 12/27/50/100 nm), and cleaving completed the processing. All devices were mounted ridge side up on copper heatsinks, and then placed into a Peltier-cooled aluminum box with an antireflection coated ZnSe window. In this box, they were held at a constant temperature between 0 and 120 °C. A commercial pulse generator (Alpes Lasers, TPG 128) with power supply (Alpes Lasers, LDD 100) allowed us to deliver 45 ns long current pulses at a variable repetition frequency to the laser. For spectral measurements, the light of the QC DFB laser was collected by an $f/1.33$ Au-coated parabolic mirror, and then bounced off a $f/3.75$ parabolic mirror to enter the 100 μm wide entrance slit of a grating spectrometer (Jobin–Yvon, $d_{\text{focal}}=0.3\,\text{m}$, $\Lambda=300\,\text{lines/mm}$). Behind the spectrometer, the light was detected with a battery-driven pyroelectric detector. For the measurement of $L-I$ curves, a calibrated thermopile detector was used; it measured the average power from one facet of the laser.

Typical $L-I$ and $I-V$ curves of a 44 μm wide and 3 mm long device are shown in Fig. 2. The 45 ns long pulses came along with a pulse repetition frequency of 333 kHz; this

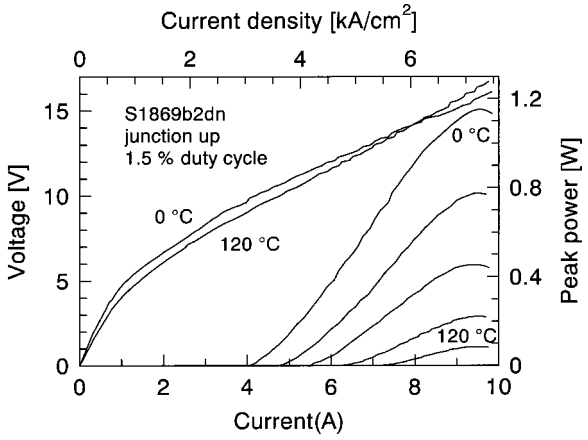

FIG. 2. $L-I$ and $I-V$ curves of a 44 μm wide and 3 mm long QC DFB laser at a wavelength of 5.3 μm. The curves were measured at a duty cycle of 1.5% and at five different temperatures between 0 and 120 °C.

corresponds to a duty cycle of 1.5%. The emitted peak power drops from 1.15 W at 0 °C via 0.45 W at 60 °C to 92 mW at 120 °C. These maximum power values come along with slope effciencies of 247 mW/A at 0 °C, 135 mW/A at 60 °C, and finally 45 mW/A at 120 °C. We observed threshold currents of 4.1 A at 0 °C, 5.6 A at 60 °C, and 7.4 A at 120 °C; these values are equivalent to threshold current densities of 3.1, 4.2, and 5.6 kA/cm^2 at the respective temperatures. The characteristic temperature, T_0, which empirically describes the behavior of the threshold current as a function of the temperature, was 203 K. As a comparison, we also fabricated Fabry–Pérot (FP) lasers from the same material, using the same lateral current injection scheme and an identical geometry. For those multimode lasers, we achieved even higher peak powers of 1.76 W at 0 °C ($dP/dI=311\,\text{mW/A}$, $j_{\text{th}}=3\,\text{kA/cm}^2$) and 0.83 W at 60 °C ($dP/dI=258\,\text{mW/A}$, $j_{\text{th}}=5.4\,\text{kA/cm}^2$). T_0 was with 190 K comparably high as for the DFB lasers. The excellent performance of both DFB and FP devices demonstrates that lateral current injection with or without surface gratings is a very effective technique for high power QC lasers.

In Fig. 3, we present the emission spectra measured at the thermal rollover point for 5 representative temperatures between 0 and 120 °C. The same pulse lengths and repetition

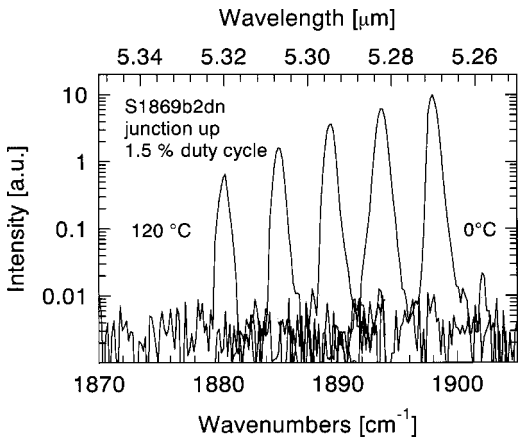

FIG. 3. Emission spectra of a 44 μm wide and 3 mm long QC DFB laser at a wavelength of 5.3 μm. The spectra were collected at the same 5 temperatures as the $L-I-V$ curves of Fig. 2 and at the thermal rollover point for each temperature.

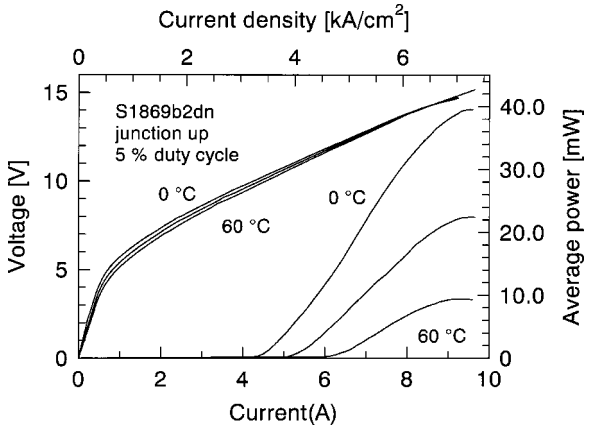

FIG. 4. $L-I$ and $I-V$ curves of a 44 μm wide and 3 mm long QC DFB laser at a wavelength of 5.3 μm. The curves were measured at a duty cycle of 5% and at three different temperatures between 0 and 60 °C.

rates as in Fig. 2 were used for this experiment. The single lasing mode tunes linearly with temperature from 1898 cm^{-1} at 0 °C to 1881 cm^{-1} at 120 °C. We thus obtained a temperature tuning rate of $\Delta k/\Delta T = -0.145\,\mathrm{cm}^{-1}/\mathrm{K}$. Because of the limited dynamical range of our setup, a correct measurement of the side mode suppression ratio (SMSR) is not possible. Keeping this fact in mind, we understand that the signal to noise ratio (SNR) of the lasing peaks in Fig. 3 is only a lower limit for the SMSR. Due to the power decrease at higher temperatures, these SNR values drop from 30 dB at 0 °C to 20 dB at 120 °C. Obviously this does not necessarily mean that the SMSR dropped also by 10 dB. The full width at half maximum linewidth of the emission peaks is on the order of 0.75 cm^{-1} for all investigated temperatures. It is obvious that thermal chirping dictates this linewidth, similar as outlined in Ref. 7. For this reason, we made experiments with a reduced pulse length (down to 20 ns) and found a linewidth on the order of 0.15 cm^{-1}.

Figure 4 shows the maximal average output power measured at three different temperatures up to 60 °C. These curves were measured using 45 ns pulses as well, but with a higher repetition frequency of 1.11 MHz; this results in a duty cycle of 5%. The highest output power was achieved at 0 °C; its value at the thermal rollover point was 39.5 mW. At room temperature, we still observed 22.5 mW, and finally, at 60 °C, the value decreased to 9.5 mW. As reported earlier on a 10.4 μm DFB laser using the same lateral contact scheme, we observed that the duty cycle yielding the highest thermal rollover power changed with temperature. This is illustrated best when dividing the average thermal rollover powers at 5% and 1.5% duty cycle for the three available temperatures. At 0 °C, the ratio $r = P_{\max}(5\%)/P_{\max}(1.5\%)$ is 2.28, at 30 °C we find $r = 1.94$, and finally at 60 °C we obtain $r = 1.38$. This shows how the laser suffers from overheating at elevated temperatures, which is understandable when taking into account the small area into which current is injected. Another indication for this overheating effect is given by the temperature tuning rate of $\Delta k/\Delta T = -0.145\,\mathrm{cm}^{-1}/\mathrm{K}$, which is somewhat larger than what has been published in the literature. In Ref. 12 for example, a value of $\Delta k/\Delta T = -0.124\,\mathrm{cm}^{-1}/\mathrm{K}$ was reported. Finally, the overheating manifests itself also in slightly higher threshold current densities, for example 3.35 $\mathrm{kA/cm}^2$ for 5% at 0 °C compared to 3.1 $\mathrm{kA/cm}^2$ for 1.5% at 0 °C. Taking into account the T_0 value from before, such an increase of the threshold current density corresponds to a temperature increase in the active region of almost 15 K.

In conclusion, we have demonstrated a single-mode QC DFB laser based on a design which combines the efficient injection of the classical 3 QW active region with diagonal transition and the short lower state lifetime of the superlattice active region with vertical transition. The device could be operated at temperatures up to 120 °C and delivered 1.15 W peak power at 0 °C.

The authors gratefully acknowledge the technical assistance of Ursula Oesterle (Ecole Polytechnique Fédérale, Lausanne, Switzerland) and Antoine Müller (Alpes Lasers SA, Neuchâtel); and the financial support of both the BRITE/EURAM project UNISEL (Contract No. CT97.0557) and the Swiss National Science Foundation.

[1] P. Repond, T. Marty, and M. W. Sigrist, Helv. Phys. Acta **65**, 828 (1992).
[2] M. Nägele, D. Hofstetter, J. Faist, and M. W. Sigrist, Proceedings of the 11th International Conference on Photoacoustic and Photothermal Phenomena, Kyoto, Japan, 2000.
[3] P. Hess, in *Principles and Perspectives of Photothermal and Photoacoustic Phenomena*, edited by A. Mandelis (Elsevier, New York, 1992), Chap. 4.
[4] B. Mizaikoff, C. S. Murthy, M. Kraft, V. Pustogow, A. Müller, D. Hofstetter, J. Faist, and N. Croitoru, Proceedings of PITTCON 2000, New Orleans, LA, 2000.
[5] C. Gmachl, F. Capasso, J. Faist, A. L. Hutchinson, A. Tredicucci, D. L. Sivco, J. N. Baillargeon, S. N. G. Chu, and A. Y. Cho, Appl. Phys. Lett. **72**, 1430 (1998).
[6] R. Köhler, C. Gmachl, A. Tredicucci, F. Capasso, D. L. Sivco, S.-N. G. Chu, and A. Y. Cho, Appl. Phys. Lett. **76**, 1092 (2000).
[7] D. Hofstetter, T. Aellen, M. Beck, and J. Faist, IEEE Photonics Technol. Lett. **12**, 1612 (2000).
[8] J. Faist, F. Capasso, D. L. Sivco, A. L. Hutchinson, S.-N. G. Chu, and A. Y. Cho, Appl. Phys. Lett. **72**, 680 (1998).
[9] J. Faist, F. Capasso, C. Sirtori, D. L. Sivco, A. L. Hutchinson, and A. Y. Cho, Appl. Phys. Lett. **66**, 538 (1995).
[10] D. Hofstetter, J. Faist, M. Beck, and U. Oesterle, Appl. Phys. Lett. **75**, 3769 (1999).
[11] D. Hofstetter, J. Faist, A. Müller, M. Beck, and U. Oesterle, Appl. Phys. Lett. **75**, 665 (1999).
[12] J. Faist, C. Gmachl, F. Capasso, C. Sirtori, D. L. Sivco, J. N. Baillargeon, and A. Y. Cho, Appl. Phys. Lett. **70**, 2670 (1997).